THE JOURNAL OF PHYSICAL CHEMISTRY C

Article

Cite This: J. Phys. Chem. C 2018, 122, 18705−18714

pubs.acs.org/JPCC

Thin-Film Texture and Optical Properties of Donor/Acceptor Complexes. Diindenoperylene/F6TCNNQ vs Alpha-Sexithiophene/F6TCNNQ

Giuliano Duva,[*,†] Linus Pithan,[‡,∥] Clemens Zeiser,[†] Berthold Reisz,[†] Johannes Dieterle,[†] Bernd Hofferberth,[†] Paul Beyer,[‡] Laura Bogula,[‡,⊥] Andreas Opitz,[‡] Stefan Kowarik,[‡,#] Alexander Hinderhofer,[*,†] Alexander Gerlach,[†] and Frank Schreiber[†,§]

[†]Institute for Applied Physics, University of Tübingen, Auf der Morgenstelle 10, 72076 Tübingen, Germany

[‡]Department of Physics, Humboldt-Universität zu Berlin, Newtonstraße 15, 12489 Berlin, Germany

[§]Center for Light-Matter Interactions, Sensors & Analytics (LISA+), Auf der Morgenstelle 15, 72076 Tübingen, Germany

[∥]ESRF—The European Synchrotron, 71, Avenue des Martyrs, 38000 Grenoble, France

[⊥]Leibniz-Institut für Kristallzüchtung, Max-Born-Straße 2, 12489 Berlin, Germany

[#]Bundesanstalt für Materialforschung und -prüfung (BAM), Unter den Eichen 44−46, 12203 Berlin, Germany

Supporting Information

ABSTRACT: In this work, two novel donor/acceptor (D/A) complexes, namely, diindenoperylene (DIP)/1,3,4,5,7,8-hexafluoro-tetracyanonaphthoquinodimethane (F6TCNNQ) and alpha-sexithiophene (6T)/F6TCNNQ, are studied. The D/A complexes segregate in form of $\pi-\pi$ stacked D/A cocrystals and can be observed by X-ray scattering. The different conformational degrees of freedom of the donor molecules, respectively, seem to affect the thin-film crystalline texture and composition of the D/A mixtures significantly. In equimolar mixtures, for DIP/F6TCNNQ, the crystallites are mostly uniaxially oriented and homogeneous, whereas for 6T/F6TCNNQ, a mostly 3D (isotropic) orientation of the crystallites and coexistence of domains of pristine compounds and D/A complex, respectively, are observed. Using optical absorption spectroscopy, we observe for each of the two mixed systems a set of new, strong transitions located in the near-IR range below the gap of the pristine compounds: such transitions are related to charge-transfer (CT) interactions between donor and acceptor. The optical anisotropy of domains of the D/A complexes with associated new electronic states is studied by ellipsometry. We infer that the CT-related transition dipole moment is perpendicular to the respective π-conjugated planes in the D/A complex.

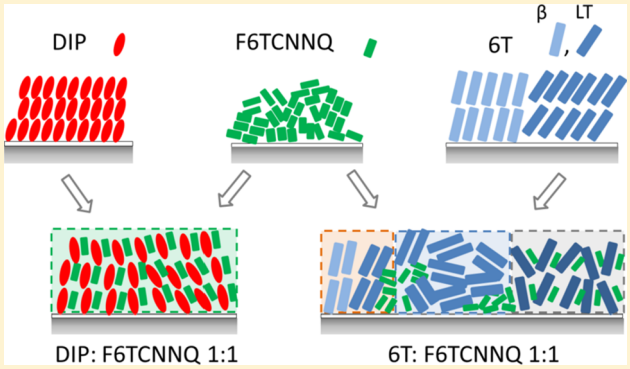

INTRODUCTION

Organic molecular semiconductors (OSCs) represent an interesting class of materials[1] for applications in several kinds of optoelectronic devices such as organic field-effect transistors, organic light-emitting diodes, and organic solar cells.[2,3] In particular, vacuum-deposited thin films of OSCs offer a wide range of possibilities for structural control.[4−6] Heterostructures can be tailored to obtain the desired material properties.[7,8]

One application of the heterostructure concept is the so-called "molecular electrical doping", namely, an organic semiconducting matrix is doped with another OSC with the aim of manipulating layer conductivity[9] by means of charge-transfer (CT) between two types of OSCs. For example, it has been observed that *N*,*N*,*N*′,*N*′-tetrakis(4-methoxyphenyl)-benzidine (MeO-TPD) undergoes integer CT (ICT) when p-doped with the widely investigated 2,3,5,6-tetrafluoro-7,7,8,8-tetracyanoquinodimethane (F4TCNQ).[10] ICT is also observed for 2,2′,7,7′-tetrakis(*N*,*N*-diphenylamino)-9,9-spirobifluorene (Spiro-TAD) doped with 1,3,4,5,7,8-hexafluoro-tetracyanonaphthoquinodimethane (F6TCNNQ),[11] the latter being less volatile and having higher electron affinity than F4TCNQ. For some linear and planar molecules, the strong coupling of the donor's highest occupied molecular orbital (HOMO) with the acceptor lowest unoccupied molecular orbital (LUMO) can lead to the formation of a hybrid molecular complex between donor and acceptor (D/A complex) with partial CT character.[12] In this case, the D/A complex itself becomes the "dopant" of the surrounding matrix.[13] Two recent works[14,15] have reviewed the different mechanisms in which molecular doping can occur. Despite the

Received: April 20, 2018
Revised: July 18, 2018
Published: July 19, 2018

DOI: 10.1021/acs.jpcc.8b03744
J. Phys. Chem. C 2018, 122, 18705−18714

numerous studies already carried out, to date only a limited number of systems has been studied; therefore, it is useful to extend the spectrum of investigated material combinations to shed more light on the microscopic mechanisms occurring within molecular D/A systems.

Because of the planar and elongated shape of the molecular semiconductors used in this work, they exhibit intrinsically anisotropic electronic properties on the molecular scale. Such anisotropy strongly impacts intermolecular coupling in the solid state. Typically, charge carrier transport and optical transitions in uniaxially oriented thin films of OSCs exhibit peculiar features when decomposed in their in-plane and out-of-plane component relative to the substrate surface. Therefore, the study of anisotropic properties in thin films of OSCs is highly relevant for devices. Examples of uniaxially anisotropic optical properties in thin films of molecular semiconductors have been reported in refs.[16−21] In these studies, the focus has been kept mainly on the optical anisotropy of one-component films, for which transitions at energies equal or above the fundamental gap (typically around 2 eV) were investigated. In heterostructures with D/A character, intermolecular interactions can give rise to several new optical transitions located below the band gap of the pristine materials. For some systems, an electronic transition from the hybrid HOMO to the hybrid LUMO in a D/A complex seems to be the origin of at least the lowest-energy transition.[22] If segregation of extended crystalline domains containing the D/A complex occurs, one can expect optical anisotropy of the new, sub-bandgap transitions as a consequence of the textured alignment of the domains containing the molecular complex in the film. In the framework of D/A complex formation in thin films of OSCs, the anisotropy of new, sub-bandgap optical transitions related to intermolecular CT has been addressed in a very recent work that contains a thorough study of the effects of CT interactions in the binary mixtures of perylene core-based OSCs.[23] There, the materials employed exhibit very similar molecular size; however, the intensity of the new transitions relative to those above the optical gap of the pristine materials was rather low.

In the study presented here, thin films were grown via vacuum deposition of two D/A couples with varying mixing ratio in a bulk heterojunction architecture to maximize the number of donor/acceptor interfaces. For both combinations, we employed the recently studied F6TCNNQ (also known as F6-TNAP)[24] as acceptor; the donor compounds are diindenoperylene (DIP)[25−27] and alpha-sexithiophene (6T).[28−30] The materials employed exhibit a planar and elongated shape and differ significantly in length. The donor molecules were chosen such that it is possible to expect for them different conformational degrees of freedom (less for DIP than for 6T). Additionally, because of the relative alignment of the donor HOMO to the acceptor LUMO, an energetically favored CT from the donors to the acceptor is expected (Figure 1). We introduce the idea that a larger number of conformational degrees of freedom of the molecular donor leads to an enhancement of thin-film 3D (isotropic) texturing as well as to partial phase-separation between donor and acceptor. Remarkably, because of the strong D/A interaction, we observe for both systems the formation of a D/A complex with corresponding segregation of D/A cocrystallites, although they lack long-range order. The formation of D/A cocrystals is deduced by structural analysis and confirmed by optical spectroscopy, the latter showing new electronic transitions in the mixtures related to D/A CT

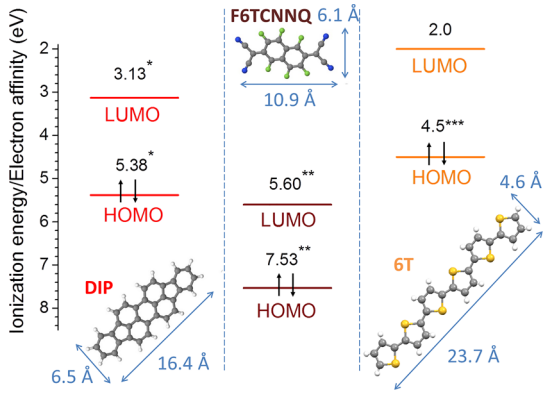

Figure 1. Energy levels of frontier orbitals and molecular structure of DIP, 6T, and F6TCNNQ. The HOMO and LUMO values were obtained from different references as peak onsets: *ref 31, from UPS and IPES measurements for standing-up molecules; **ref 11, from UPS and IPES measurements; ***from ref 32, from UPS measurements for standing-up molecules (the LUMO position of 6T was calculated from its HOMO onset with an estimated transport gap of 2.5 eV[33]).

interactions within the cocrystals. These bands peak at energies specific to the material combination. Finally, the correlation of the optical anisotropy of the new CT transitions with the orientation of the cocrystallites on the substrate allows one to conclude that the transition dipole moment (TDM) associated with the new optical transitions is oriented perpendicular to the π-conjugated planes of the face-to-face stacked donor and acceptor molecules within the complex.

In presenting our results, we first compare X-ray scattering data for DIP/F6TCNNQ and 6T/F6TCNNQ mixtures, respectively, with focus on the mixtures in 1:1 M ratio. We then compare optical absorption spectroscopy data for these 1:1 mixtures with data for the pristine compounds and finally we focus on the optical anisotropy of the equimolar mixtures.

EXPERIMENTAL SECTION

F6TCNNQ was purchased from Novaled. DIP was purchased from Institut für PAH Forschung (Greifenberg, Germany). 6T was purchased from Sigma-Aldrich. F6TCNNQ and DIP were used without further purification, whereas 6T was further purified via vacuum sublimation. The lengths of the long and short molecular axis (Figure 1), respectively, have been extracted from the crystallographic structural data of DIP[27] (long axis: distance between terminal hydrogens; short axis: distance between central hydrogens) and 6T[34] (long axis: distance between terminal hydrogens; short axis: distance between opposite hydrogens bonded to two adjacent thiophene rings) using the software Mercury.[35] For F6TCNNQ, the length of the long and short molecular axis, respectively, has been obtained from a density functional theory (DFT) calculation (long axis: distance between terminal nitrogens; short axis: distance between central fluorines).

Thin films were grown via thermal sublimation in a vacuum chamber with a base pressure of $2-4 \times 10^{-8}$ mbar. As substrates Si with both a native and a thermal oxide layer (the latter 121 nm thick) as well as borosilicate glass (Borofloat) were used. Prior to growth of the organic films, the substrates were cleaned first with acetone and then with isopropanol in an ultrasonic bath and immediately dried under a gentle flow of

DOI: 10.1021/acs.jpcc.8b03744
J. Phys. Chem. C 2018, 122, 18705−18714

N_2; the substrates were subsequently heated up to 523 K for 2 h in vacuum before film deposition. During the growth, they were kept at 300 K. Films of the pristine compounds as well as DIP/F6TCNNQ and 6T/F6TCNNQ mixtures in different mixing ratios were grown. In the mixed films, the molar ratio of one species with respect to the other was varied by adjusting the relative growth rates, keeping the total growth rate between 0.15 and 0.3 nm/min. The growth rates were monitored with two separate quartz crystal microbalances (for donor and acceptor materials, respectively) calibrated by X-ray reflectivity for DIP and 6T and by atomic force microscopy (AFM) for F6TCNNQ. The error on the mixing ratios is estimated to be ±10%.

X-ray surface scattering measurements were carried out at synchrotron facilities. The data presented were acquired ex situ at the I07 beamline[36] of the Diamond Light Source (DLS, Oxford, United Kingdom) and at the ID03 beamline of the European Synchrotron Research Facility (ESRF, Grenoble, France). Reflectivity (XRR) and Grazing-Incidence (GIXD) geometries were used to investigate the film structure in the direction perpendicular (Q_z) and parallel ($Q_{||}$) to the substrate, respectively. 2D detectors were used for X-ray scattering measurements: a Pilatus 100K[37] at the I07 beamline and a Maxipix 2 × 2 at the ID03 beamline. The beam energy was 13 keV at I07 and 18 keV at ID03.

UV−vis−NIR absorption data were collected using two different instruments in transmission geometry: a Cary 50 UV−vis spectrophotometer (Varian) for spectra with photon energy down to 1.25 eV and a Cary 5000 UV−vis−NIR spectrophotometer (Varian) for the spectra with energy down to 0.375 eV (because of absorption of the glass,[38] information about the organic films can be extracted only above ∼0.5 eV). Thin films with different D/A mixing ratios were measured down to 1.25 eV, as shown in the Supporting Information, Figure S4. Thin films in a mixing ratio of 1:1 as well as the pristine compounds were measured down to 0.375 eV to show also the lowest energy transitions.

A Woollam M-2000 spectroscopic ellipsometer with extended range in the NIR (676 wavelengths in total for a spectral range between 5 and 0.75 eV) was used to get information about the optical anisotropy of the films. The samples were measured in both transmission and reflection geometry using the same nominal sample (i.e., same growth process) grown on Si with both a native and a thermal oxide layer and on borosilicate glass, allowing for a multisample analysis.[19] Ellipsometric measurements in reflection were performed with incidence angles of 45° to 80° in steps of 5°, and in transmission between 0° and 70° in steps of 5° (angles are with respect to the substrate normal). Simple transmittance measurements with polarized light were also performed with this instrument on the samples grown on borosilicate glass to increase the robustness of the data fit. Data were analyzed using the software WVASE.[39] To account for the top roughness of the thin films in the ellipsometry fit, we applied an effective medium approximation (EMA) in our model.

AFM scans were acquired in tapping mode with a Nanowizard II (JPK Instruments) AFM. Scans are shown in Figures S7 and S8 and discussed in the Supporting Information.

RESULTS AND DISCUSSION

X-ray Scattering. In Figures 2 and 3, X-ray scattering data of DIP/F6TCNNQ and 6T/F6TCNNQ mixtures on native Si oxide are shown. We distinguish Bragg peaks from the pristine compounds and Bragg peaks in the mixtures that stem presumably from a D/A cocrystal. We first focus on the results for the DIP/F6TCNNQ series. Then, we illustrate the results for the 6T/F6TCNNQ series. Bragg peaks found in XRR and GIXD scans are summarized in Tables S1 and S2 of the Supporting Information, where we also provide a more detailed discussion of the X-ray scattering data. From the XRR scans of the DIP/F6TCNNQ series (Figure 2a), we see that Bragg peaks characteristic of a standing-up (σ) orientation of DIP[27] are broadening and then disappearing as the relative amount of the acceptor F6TCNNQ increases in the films. At the same time, new Bragg peaks arise which do not belong to pristine DIP. Pristine F6TCNNQ does not exhibit any significant out-of-plane order; therefore, it is unlikely that the new peaks stem from segregated F6TCNNQ domains. The new peaks are attributed to a DIP/F6TCNNQ D/A cocrystal. In particular, the peak at Q_z = 0.67 Å^{-1} for the 1:1 mixture (corresponding to a distance of ∼9.4 Å in real space) could

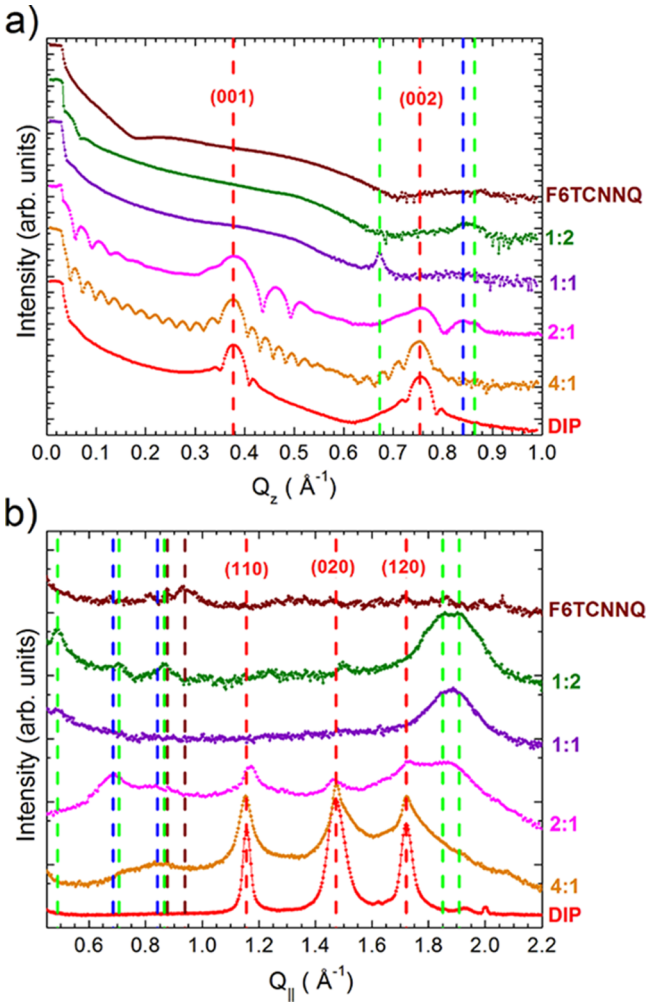

Figure 2. (a) XRR and (b) GIXD scans for D/A mixtures with DIP as donor and F6TCNNQ as acceptor mixed in different molar ratios. Vertical dashed lines show the peak attribution: [red] DIP thin-film polymorph, [blue] DIP low-T or other polymorph, [brown] F6TCNNQ, and [green] DIP/F6TCNNQ D/A cocrystal. The Miller indexes of the Bragg peaks for the DIP thin-film polymorph are shown. The film thicknesses are 23 nm (pristine DIP), 30 nm (4:1), 30 nm (2:1), 14 nm (1:1), 22 nm (1:2), and 31 nm (pristine F6TCNNQ).

DOI: 10.1021/acs.jpcc.8b03744
J. Phys. Chem. C 2018, 122, 18705−18714

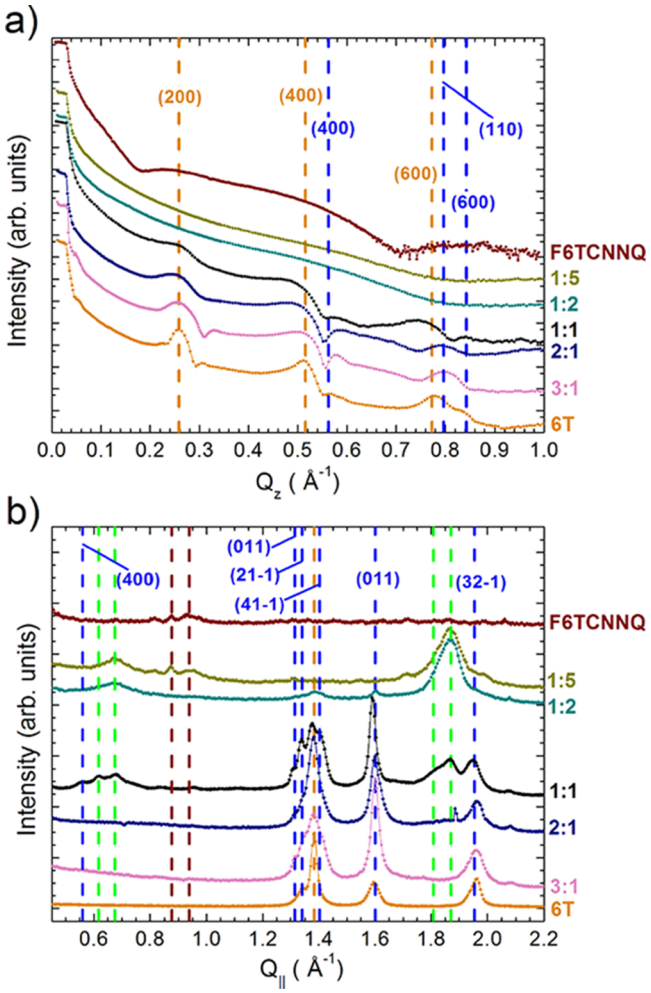

Figure 3. (a) XRR and (b) GIXD scans for D/A mixtures with 6T as donor and F6TCNNQ as acceptor mixed in different molar ratios. Vertical dashed lines show the peak attribution: [orange] 6T β polymorph, [blue] 6T low-T polymorph, [brown] F6TCNNQ, and [green] 6T/F6TCNNQ D/A cocrystal. The Miller indexes of the Bragg peaks for the 6T low-T polymorph are shown. The film thicknesses are 24 nm (pristine 6T), 27 nm (3:1), 25 nm (2:1), 72 nm (1:1), 23 nm (1:2), 27 nm (1:5), and 31 nm (pristine F6TCNNQ).

stem from a highly tilted edge-on orientation of the D/A stacks within the new cocrystal unit cell, similar to what observed for a naphtho[1,2-*b*:5,6-*b*′]dithiophene/F6TCNNQ D/A cocrystal introduced recently in ref 40. For the mixtures with excess DIP, one clearly observes a smoothing effect (enhanced Kiessig oscillations at low Q_z values) compared with the pristine DIP, as already observed for instance in DIP/C_{60} mixtures.[41,42] As the amount of F6TCNNQ increases, the films get rougher, although some weak Kiessig oscillations are still visible. For pristine F6TCNNQ, the Kiessig oscillations at low Q_z are absent, but the reflectivity curve exhibits a very broad hump, which might indicate the presence of a wetting F6TCNNQ monolayer on the Si oxide surface.

From the GIXD profiles (Figure 2b), we observe marked changes as the relative amount of F6TCNNQ in the films increases. The peaks stemming from (σ)-DIP tend to broaden and then disappear in the mixtures with higher relative amount of F6TCNNQ. At the same time, new features appear in the scans. The most pronounced changes consist of the broad peaks arising between 1.80 and 1.95 Å^{-1} in $Q_{||}$. A new pronounced peak appears also at 0.49 Å^{-1}. We attribute all these new features to a D/A DIP/F6TCNNQ cocrystal. The peak at 0.49 Å^{-1}, for example, might stem from the distance between adjacent inequivalent D/A stacks.[40] A number of additional peaks appear in the region 0.6−1 Å^{-1} for the mixed films. Although an obvious attribution could not be found, an assignment was attempted based on considerations reported in the Supporting Information.

We consider now the XRR (Figure 3a) and GIXD (Figure 3b) scans for the 6T/F6TCNNQ series. Similar to the XRR of the DIP/F6TCNNQ series, the Bragg peaks of standing-up 6T (present in both low-temperature (LT) and β phase[43,44]) broaden and then disappear with increasing relative amount of F6TCNNQ. The tendency to randomization of the orientation of the crystalline domains in the mixtures with excess F6TCNNQ is therefore a common feature of both D/A systems. In the films with excess 6T, though, we do not observe any smoothing. The GIXD profiles of the mixtures from 3:1 to 1:1 show that the (41−1) Bragg peak gets stronger. Also, in the GIXD of the 1:1 mixture, the (400) peak of the 6T LT phase appears. The presence of these features in the in-plane scans indicates that even in the equimolar blend, 6T tends to segregate in crystalline domains that have a more random orientation compared with pristine 6T films as the content of F6TCNNQ increases, an effect which was not observed in the DIP/F6TCNNQ series. In the 6T/F6TCNNQ series it is also possible to observe the development of new peaks in the region $Q_{||}$ = 1.80−1.95 Å^{-1}, together with a new peak at 0.67 Å^{-1}. Therefore, for 6T/F6TCNNQ, one can also deduce the formation of D/A cocrystals.

The new features in the GIXD scans appearing at similar values of $Q_{||}$ between 1.80 and 1.95 Å^{-1} for both series of mixtures likely stem from crystallographic directions vicinal to or coincident with the $\pi-\pi$ donor−acceptor stacking direction, as illustrated in the Supporting Information by comparison of some GIXD scans with the powder diffraction patterns of known D/A compounds (Figures S2 and S3). We therefore suggest that both DIP/F6TCNNQ and 6T/F6TCNNQ pairs form D/A stacks, which usually results in some degree of CT interaction as observed for other D/A pairs.[45−48]

In Figure 4, we show the reciprocal space maps (i.e., full diffraction patterns) measured for DIP/F6TCNNQ (100 nm) and 6T/F6TCNNQ (72 nm) 1:1 mixtures. Overall, the diffracted intensity from the D/A cocrystal features appears in the *Q*-space as either elongated spots with some angular distribution or as Debye−Scherrer rings. The elongated spots for DIP/F6TCNNQ (Figure 4a) indicate a mostly uniaxial arrangement of the molecular D/A crystalline domains (i.e., in the fashion of a 2D textured powder) although with some mosaicity on the order of ∼40° (see angular distribution of the integrated intensity of the diffraction features ascribed to the respective cocrystals in the Supporting Information, Figure. S1). The intensity of the diffraction features with $Q_{||}$ = 1.80−1.95 Å^{-1} (corresponding in real space to a $\pi-\pi$ stacking distance of 3.5−3.2 Å) is mostly concentrated in the region of low Q_z near the total reflection edge of the samples. This indicates that the direction of the $\pi-\pi$ stacking of the D/A molecular components is roughly parallel to the substrate plane. For 6T/F6TCNNQ (Figure 4b), the diffraction features with $Q_{||}$ = 1.80−1.95 Å^{-1} appear as diffraction rings of uniformly distributed intensity; therefore, it is not possible to deduce a preferred orientation of the π-stacking direction with

DOI: 10.1021/acs.jpcc.8b03744
J. Phys. Chem. C 2018, 122, 18705−18714

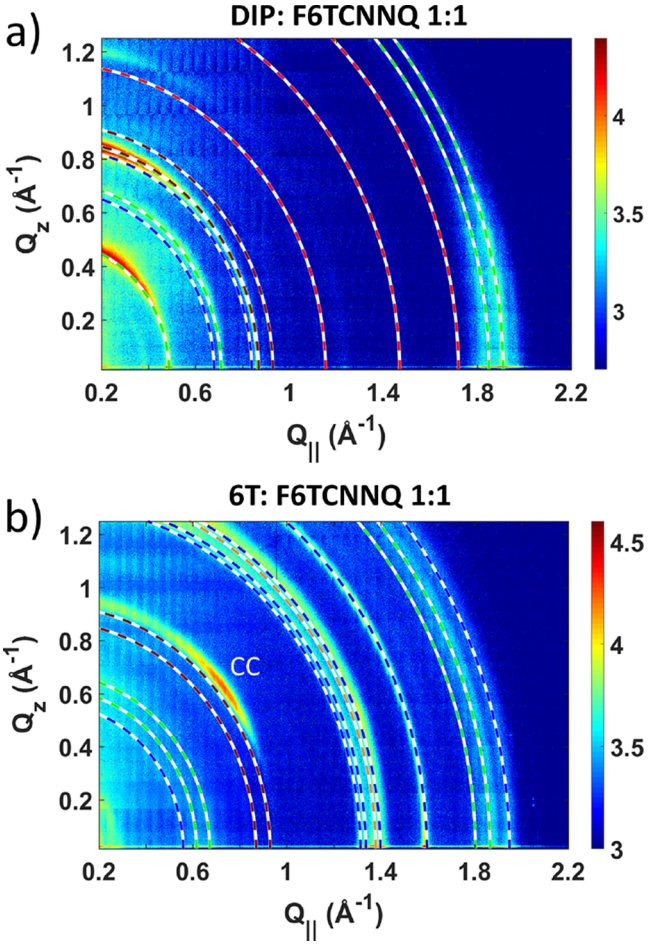

Figure 4. Reciprocal space maps of (a) DIP/F6TCNNQ (thickness: 100 nm) and (b) 6T/F6TCNNQ (thickness: 72 nm) 1:1 mixtures grown on native Si oxide. Color bars in logarithmic scale. Dashed lines indicate Debye−Scherrer rings whose total Q corresponds to the GIXD peaks in Figures 2b and 3b respecting the same color code. For the 6T/F6TCNNQ 1:1 mixture, the diffraction feature exhibiting a maximum at $Q_{||} \approx 0.73$ Å^{-1}, $Q_z \approx 0.62$ Å^{-1} and marked "CC" is also assigned to the cocrystal, but its component along the $Q_z = 0$ Å^{-1} direction is too weak and therefore it is not marked in the corresponding GIXD scan of Figure 3b.

respect to the substrate plane for this system. However, the elongated spot at $Q_{||} \approx 0.73$ Å^{-1}, $Q_z \approx 0.62$ Å^{-1} assigned to the cocrystal (marked with "CC") indicates some preferred orientation. Because of the lack of knowledge about the crystal structure of the two D/A complexes, indexing of the Bragg peaks is prohibitive. Overall, we conclude that DIP/F6TCNNQ cocrystallites have a tendency for 2D powder-like texture with large mosaicity, whereas 6T/F6TCNNQ cocrystallites have a tendency for 3D powder arrangement. We explain this effect invoking additional degrees of freedom of the longer 6T molecule (e.g., flexibility as in the case simulated for *para*-sexiphenyl[49] or interannular torsion angles[50]) compared with the shorter and stiffer DIP: this might involve a high concentration of defects incorporated in a growing 6T/F6TCNNQ molecular layer, rendering the growth of the subsequent layers more disordered and isotropic. Note that this mechanism can explain also the absence of film smoothing for the 6T/F6TCNNQ mixtures with nominal excess of 6T compared with the DIP/F6TCNNQ mixtures with nominal excess of DIP, where smoothing is observed (Figures 2a and 3a). However, such explanation is still on the level of hypothesis, which is intrinsically hard to prove.

Diffraction features belonging to crystallites of the pristine donor DIP are virtually absent in the reciprocal space map of the DIP/F6TCNNQ 1:1 mixture, whereas for the 6T/F6TCNNQ 1:1 mixture, one can clearly recognize the features of pristine 6T crystallites (F6TCNNQ in pristine films is only weakly crystalline and we do not observe diffraction stemming from segregated F6TCNNQ domains in the mixed films closer to a 1:1 mixing ratio). We speculate that for 6T/F6TCNNQ the difference in free energy between D/A cocrystallites and phase-separated domains of the pristine compounds is rather small because of the conformational degrees of freedom of 6T as highlighted above. Therefore, kinetic effects[42] and inhomogeneities in the surface potential landscape, for example, defects, might play a dominant role in determining which phase nucleates locally. The deduced structure and mixing behavior in the D/A mixtures of the compounds studied here is sketched in Figure 5.

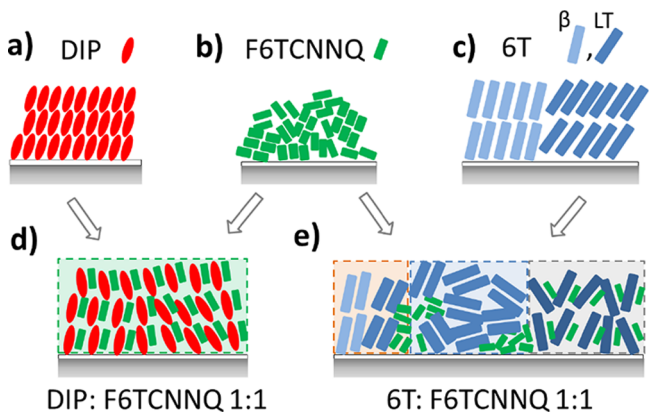

Figure 5. Sketches of the structure of the pristine compounds and D/A mixtures in thin films on native and thermal Si oxide. (a) DIP, standing-up. (b) F6TCNNQ, no long-range crystalline order. (c) 6T, standing up, with β phase and low-T phase exhibiting different tilt angle of the long molecular axis with respect to the substrate plane. (d) DIP/F6TCNNQ 1:1, homogeneous distribution of D/A cocrystals. (e) 6T/F6TCNNQ 1:1, more pronounced 3D powder-like texture (gray box); partial phase separation of pristine 6T and F6TCNNQ (orange and blue boxes) and randomly oriented 6T domains (blue box).

UV−Vis−NIR Absorption Spectroscopy. In Figure 6, we present the in-plane extinction coefficient k_{xy} obtained from transmission measurements in the UV−vis−NIR region for the pristine compounds as well as for 1:1 mixtures grown on borosilicate glass. Note that because of the normal incidence of the beam, only the in-plane component of k is probed.

The optical spectra of both equimolar mixtures exhibit highly convoluted profiles in the region above ∼2 eV, which cannot be trivially reproduced by a linear combination of the spectra of the pristine compounds. For DIP/F6TCNNQ 1:1, the maximum is located around 2.4 eV, whereas for 6T/F6TCNNQ 1:1, it is located approximately at 2.8 eV. Both types of mixtures exhibit new absorption bands that lie energetically below the optical gaps (here considered as the first absorption maximum) of the pristine materials. The position and integrated intensity of all new absorption bands for both material combinations are summarized in Table 1. It is possible to fit three new peaks for the DIP/F6TCNNQ 1:1

DOI: 10.1021/acs.jpcc.8b03744
J. Phys. Chem. C 2018, 122, 18705−18714

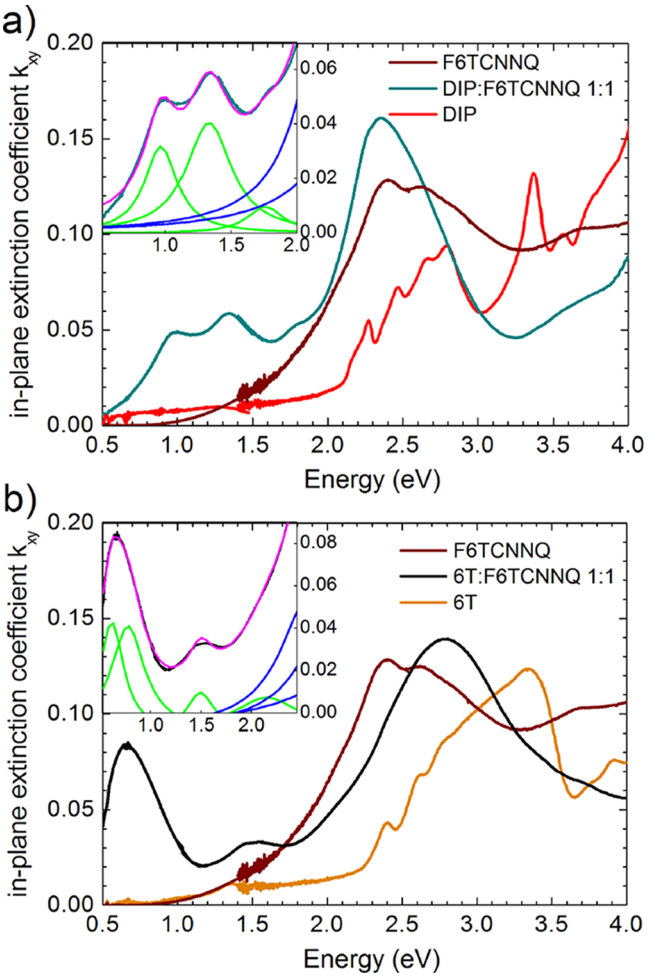

Figure 6. In-plane extinction coefficient of (a) DIP (25 nm), F6TCNNQ (13 nm), and DIP/F6TCNNQ 1:1 (103 nm) and (b) 6T (24 nm), F6TCNNQ (13 nm), and 6T/F6TCNNQ 1:1 (23 nm), all samples grown on borosilicate glass. The insets show Lorentzian fits to the new CT transitions in the 1:1 mixtures: sub-bandgap transitions (green), transitions above the gap of the pristine materials (blue), global fit (magenta). The spectral portions measured with two different instruments are reported with some overlap around 1.5 eV. The downward bending of the spectral profiles of the pristine donor compounds around 1.5 eV is an artifact due to the grating and detector changeover in the spectrometer. Note that the magnitude of k_{xy} for DIP[51,52] and for 6T[21,53] compares very well with the literature.

mixture and four for the 6T/F6TCNNQ 1:1 mixture arising below the band gap of the pristine compounds (Figure S5).

The shape, position, and relative cross sections of the new sub-bandgap absorption features are specific to the respective D/A system. We assume that all these new transitions are related to excited-state CT interactions. There is usually a close relationship between CT interactions in the excited state, as probed by UV−vis−NIR absorption, and ground-state CT interactions. To quantify the degree of CT in the ground-state in D/A cocrystals, vibrational spectroscopies like Raman scattering can be used:[54−56] results from Raman scattering for the two systems studied here are reported in the Supporting Information. However, a detailed explanation of the mechanisms that govern D/A interactions as well as a quantitative determination of the degree of CT go beyond the scope of this work. Some general considerations may nevertheless help understanding qualitatively the observed

Table 1. Energy Position and Integrated Intensity of the New Sub-bandgap Absorption Peaks in DIP/F6TCNNQ and 6T/F6TCNNQ 1:1 Mixtures[a]

mixture	energy (eV)	integr. intensity (10^{-2})
DIP/F6TCNNQ	0.97	1.5
	1.33	2.7
	1.76	0.5
6T/F6TCNNQ	0.61	1.5
	0.78	2.0
	1.49	0.5
	2.15	1.2

[a]The data were fitted using a sum of Lorentzian curves (Figures 6a,b and S5).

spectral features. In general, upon the formation of a D/A complex, the molecular orbitals of the isolated donor and acceptor are coupled to each other to some extent and therefore experience a perturbation in their shape and energy. Signatures of this coupling in optical spectra are (a) changes of the spectral profile above the optical gap of the pristine materials which cannot be reproduced by combination of the optical functions of pristine donor and acceptor according to effective medium models;[57] (b) appearance of new transitions located below the optical band gap of the pristine materials.[12,13,57,58] For the two D/A systems studied in this work, case (b) is evident. Keeping the acceptor material fixed (F6TCNNQ in our case), the characteristics of the new transitions depend on the energy and shape of the donor orbitals and on the details of the D/A coupling. These features differ significantly in DIP/F6TCNNQ compared with 6T/F6TCNNQ. Indeed, as seen from Figure 1, the long molecular axis of DIP is ∼30% longer than that of F6TCNNQ, whereas 6T is roughly twice the length of F6TCNNQ. Some DFT studies[59,60] of the free energy of isolated CT complexes as a function of the adsorption geometry (e.g., relative shifts along the molecular backbone) showed that there is only one absolute conformational minimum, although several local minima are calculated. In our study, the 6T/F6TCNNQ complex might be present in more than one conformation because of nonequilibrium kinetic effects. Additionally, in ref 59, it is reported that the coupling of the 6T HOMO with the F4TCNQ LUMO determines the HOMO−LUMO gap for the minimum-energy conformation of the 6T/F4TCNQ CT complex. The isotropic texture of the 6T/F6TCNNQ crystallites and the substructure of the strong lowest-energy optical transition in the 1:1 mixture seem to agree with the presence of several conformations of the D/A complex.

Despite the intrinsic complexity of D/A coupling in molecular materials, in the framework of molecular doping, we conclude that the origin of the lowest energy absorption feature observed for the DIP/F6TCNNQ (0.97 eV) and the 6T/F6TCNNQ (0.61 eV) 1:1 mixtures resides in the transition of one electron from a strongly hybridized HOMO to a strongly hybridized LUMO of the new D/A supramolecular complex.[12,13] We assume that the new transitions observed for these two D/A couples do not stem from fully ionized donor and acceptor species because there are no clear spectral signatures of the DIP cation (Figure S6) or 6T cation[61] together with the F6TCNNQ anion.[11] Therefore, the two material combinations studied here seem to belong to the category of D/A pairs of molecular semiconductors exhibiting partial CT in the ground state.

DOI: 10.1021/acs.jpcc.8b03744
J. Phys. Chem. C 2018, 122, 18705−18714

Ellipsometry. From X-ray scattering data, an overall 2D-texturing of the D/A cocrystallites in the 1:1 mixtures of both systems was deduced, with a more pronounced tendency to 3D-texturing for 6T/F6TCNNQ than for DIP/F6TCNNQ. Now, we investigate the uniaxial anisotropy of the new CT transitions using spectroscopic ellipsometry. In Figure 7, the results for the in-plane and out-of-plane component of the extinction coefficient for DIP/F6TCNNQ and 6T/F6TCNNQ 1:1 mixtures are shown. The results for the refractive index are reported in Figure S9. Because of the experimental setup, the spectral range of ellipsometric measurements is more restricted than for optical absorption measurements.

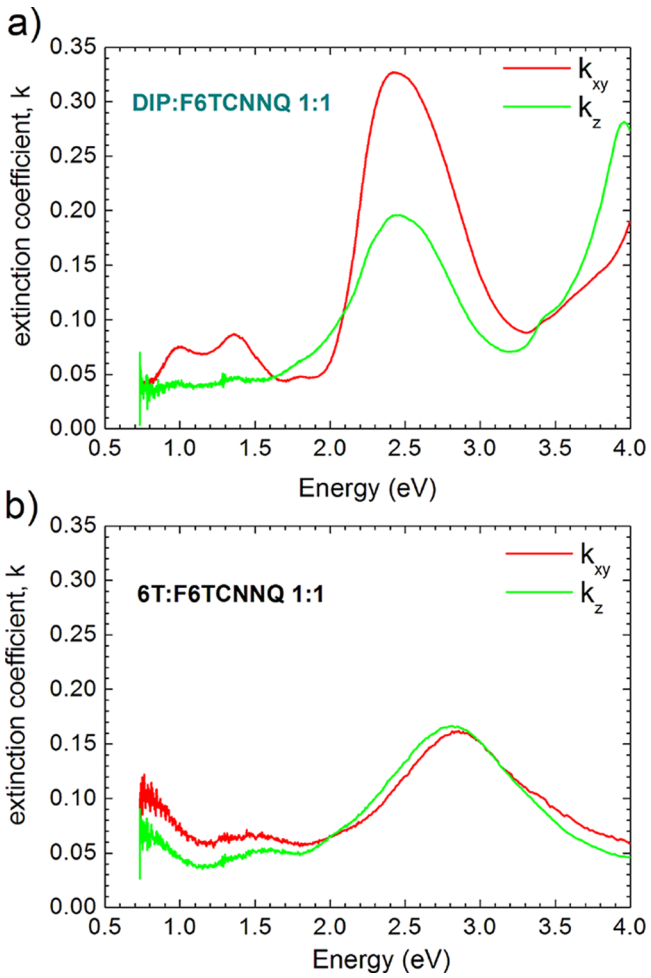

Figure 7. In-plane (k_{xy}) and out-of-plane (k_z) component of the extinction coefficient obtained from ellipsometry for (a) DIP/F6TCNNQ 1:1 (103 nm) and (b) 6T/F6TCNNQ 1:1 (23 nm) mixtures grown on Si oxide.

We modeled the ellipsometric data using a multisample analysis.[19] For the DIP/F6TCNNQ 1:1 sample, we used the films deposited on native and thermal Si oxide; for the 6T/F6TCNNQ 1:1 sample, we used the films deposited on native Si oxide and borosilicate glass. The roughness of the organic film is accounted for by including an EMA layer. The choice of the model was guided by AFM scans of the film surface, as detailed in the Supporting Information. From Figure 7, the anisotropy of the optical transitions becomes apparent. In the region above ~2 eV, the relative magnitude between k_{xy} and k_z is different for the two D/A systems, respectively. For the DIP/F6TCNNQ 1:1 film, the in-plane component is stronger across almost the whole spectrum. For the 6T/F6TCNNQ 1:1 film, in the same spectral region there is barely any difference between the two components. In the region where the new CT transitions are more clearly visible (i.e., $E < 2$ eV) the in-plane component is larger than the out-of-plane component for both mixtures, an exception being the weak band of DIP/F6TCNNQ at 1.76 eV. However, in the 6T/F6TCNNQ 1:1 mixture, the spectral shapes of the two components are very similar down to the partially visible lowest-energy transition. Conversely, k_{xy} in the DIP/F6TCNNQ 1:1 mixture exhibits pronounced maxima, whereas k_z is nearly flat. Overall, the optical anisotropy in the DIP/F6TCNNQ 1:1 mixture is more pronounced than in the 6T/F6TCNNQ 1:1 mixture, which is in agreement with the conclusions from X-ray scattering. The results for DIP/F6TCNNQ 1:1 on glass are in general agreement with the UV−vis−NIR absorption measurements (Figure S10).

For the more uniaxially anisotropic DIP/F6TCNNQ 1:1 mixture, we concluded from X-ray scattering that the direction of the D/A π-stacking within the cocrystallites is roughly parallel to the substrate plane. In the present section, we saw that the in-plane component of the new CT transitions is stronger than the out-of-plane component. Therefore, we conclude that the CT-associated TDM must be along the π-stacking direction, as already suggested for the weakly interacting D/A couple DIP/PDIR-CN_2.[23] This can be qualitatively explained by the strong CT between donor and acceptor molecules that allows strong dipoles in both the ground state and the excited state along the π-stacking direction (Figure 8). Although the 6T/F6TCNNQ 1:1 mixture does not exhibit a degree of structural anisotropy that allows one to make conclusions about the direction of the D/A π-stacking with respect to the substrate plane, an analogous picture for the orientation of the TDM seems likely.

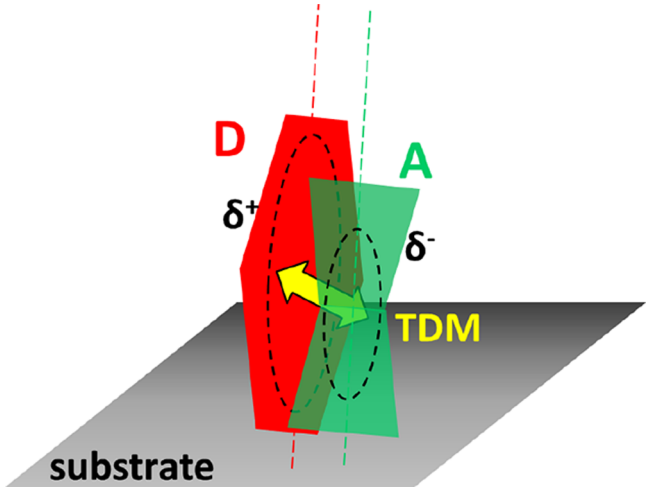

Figure 8. Sketch of the donor (D)/acceptor (A) π-stacking direction and CT TDM oriented mostly parallel to the substrate for edge-on orientation. Leading to a stronger in-plane component of the CT-related optical transitions. The "$\delta^{+/-}$" depict the partial CT of an electron from the donor to the acceptor in the ground state. The dashed ellipsoids drawn inside the molecules represent the π-conjugation. The vertical dashed lines indicate the long molecular axis. The yellow arrow indicates both the π-stacking direction and the CT TDM.

DOI: 10.1021/acs.jpcc.8b03744
J. Phys. Chem. C 2018, 122, 18705−18714

CONCLUSIONS

In conclusion, we studied two novel D/A systems of small-molecular OSCs, namely, DIP/F6TCNNQ and 6T/F6TCNNQ. We speculate that the differences in the crystalline texture and phase-composition between DIP/F6TCNNQ and 6T/F6TCNNQ equimolar mixtures, respectively, can be ascribed to the different conformational degrees of freedom of the donors. Formation of a D/A cocrystal is observed for both systems: one main driving force for cocrystal formation is the strong CT interaction between the donor and acceptor because of the energy difference between HOMO and LUMO levels. The strength of the CT interaction for these systems is further evidenced by optical absorption measurements that reveal pronounced, low-energy absorption features in the D/A 1:1 mixtures which are absent in the pristine compounds. For the more uniaxially ordered DIP/F6TCNNQ 1:1 mixture, study of the optical anisotropy reveals that the in-plane component of the extinction coefficient of the new CT absorptions is stronger than the out-of-plane component. For the 6T/F6TCNNQ 1:1 mixture exhibiting a mostly 3D powder-like texture, the optical anisotropy is less pronounced. This supports a picture in which the CT TDM is oriented along the D/A π-stacking direction. We suggest such a scenario to be rather general for D/A pairs of planar molecular semiconductors forming supramolecular complexes. In addition, the two D/A pairs studied here constitute an example of strong CT complexes that by virtue of their low-energy transitions might be employed as technologically relevant materials such as light-harvesters for NIR detectors.

ASSOCIATED CONTENT

Supporting Information

The Supporting Information is available free of charge on the ACS Publications website at DOI: 10.1021/acs.jpcc.8b03744.

Supporting Information containing: (a) additional comments to the interpretation of the X-ray scattering data; (b) UV−vis absorption spectra of DIP/F6TCNNQ and 6T/F6TCNNQ blends in mixing ratios different from the 1:1; (c) Raman scattering data of thin films on native Si oxide; (d) AFM scans of the 1:1 films on native Si oxide, thermal Si oxide and glass; (e) additional ellipsometry data; and (f) additional comments about CT interactions (PDF)

AUTHOR INFORMATION

Corresponding Authors

*E-mail: giuliano.duva@uni-tuebingen.de (G.D.).
*E-mail: alexander.hinderhofer@uni-tuebingen.de (A.H.).

ORCID

Giuliano Duva: 0000-0001-9492-3276
Andreas Opitz: 0000-0002-3214-8398
Alexander Hinderhofer: 0000-0001-8152-6386

Notes

The authors declare no competing financial interest.

ACKNOWLEDGMENTS

We thank the Diamond Light Source (UK), in particular Chris Nicklin and Jonathan Rawle, and the European Synchrotron Research Facility (FR) for providing synchrotron radiation. We thank Reinhard Scholz for the DFT calculations on F6TCNNQ and Marcus Scheele for access to the Cary 5000 spectrophotometer. We are grateful for experimental support from H.S.S. Ramakrishna Matte. The support from the DFG (projects SCHR700/20-1, OP159/2-1) is gratefully acknowledged. G.D. acknowledges the support from the Carl-Zeiss-Stiftung.

REFERENCES

(1) Brütting, W.; Adachi, C. *Physics of Organic Semiconductors*, 2nd ed.; Brütting, W., Adachi, C., Eds.; Wiley VCH-Verlag: Weinheim, 2012.

(2) Forrest, S. R. The Path to Ubiquitous and Low-Cost Organic Electronic Appliances on Plastic. *Nature* **2004**, *428*, 911−918.

(3) Sirringhaus, H.; Tessler, N.; Friend, R. H. Integrated Optoelectronic Devices Based on Conjugated Polymers. *Science* **1998**, *280*, 1741−1744.

(4) Forrest, S. R. Ultrathin Organic Films Grown by Organic Molecular Beam Deposition and Related Techniques. *Chem. Rev.* **1997**, *97*, 1793−1896.

(5) Walzer, K.; Maennig, B.; Pfeiffer, M.; Leo, K. Highly Efficient Organic Devices Based on Electrically Doped Transport Layers. *Chem. Rev.* **2007**, *107*, 1233−1271.

(6) Witte, G.; Wöll, C. Molecular Beam Deposition and Characterization of Thin Organic Films on Metals for Applications in Organic Electronics. *Phys. Status Solidi A* **2008**, *205*, 497−510.

(7) Hinderhofer, A.; Schreiber, F. Organic-Organic Heterostructures: Concepts and Applications. *ChemPhysChem* **2012**, *13*, 628−643.

(8) Opitz, A.; Wilke, A.; Amsalem, P.; Oehzelt, M.; Blum, R.-P.; Rabe, J. P.; Mizokuro, T.; Hörmann, U.; Hansson, R.; Moons, E.; et al. Organic Heterojunctions: Contact-Induced Molecular Reorientation, Interface States, and Charge Re-Distribution. *Sci. Rep.* **2016**, *6*, 21291.

(9) Lüssem, B.; Tietze, M. L.; Kleemann, H.; Hoßbach, C.; Bartha, J. W.; Zakhidov, A.; Leo, K. Doped Organic Transistors Operating in the Inversion and Depletion Regime. *Nat. Commun.* **2013**, *4*, 2775.

(10) Li, J.; Rochester, C. W.; Jacobs, I. E.; Friedrich, S.; Stroeve, P.; Riede, M.; Moulé, A. J. Measurement of Small Molecular Dopant F4TCNQ and C60F36 Diffusion in Organic Bilayer Architectures. *ACS Appl. Mater. Interfaces* **2015**, *7*, 28420−28428.

(11) Zhang, F.; Kahn, A. Investigation of the High Electron Affinity Molecular Dopant F6-TCNNQ for Hole-Transport Materials. *Adv. Funct. Mater.* **2018**, *28*, 1703780.

(12) Salzmann, I.; Heimel, G.; Duhm, S.; Oehzelt, M.; Pingel, P.; George, B. M.; Schnegg, A.; Lips, K.; Blum, R.-P.; Vollmer, A.; et al. Intermolecular Hybridization Governs Molecular Electrical Doping. *Phys. Rev. Lett.* **2012**, *108*, 035502.

(13) Méndez, H.; Heimel, G.; Winkler, S.; Frisch, J.; Opitz, A.; Sauer, K.; Wegner, B.; Oehzelt, M.; Röthel, C.; Duhm, S.; et al. Charge-Transfer Crystallites as Molecular Electrical Dopants. *Nat. Commun.* **2015**, *6*, 8560.

(14) Salzmann, I.; Heimel, G. Toward a Comprehensive Understanding of Molecular Doping Organic Semiconductors (Review). *J. Electron Spectrosc. Relat. Phenom.* **2015**, *204*, 208−222.

(15) Salzmann, I.; Heimel, G.; Oehzelt, M.; Winkler, S.; Koch, N. Molecular Electrical Doping of Organic Semiconductors: Fundamental Mechanisms and Emerging Dopant Design Rules. *Acc. Chem. Res.* **2016**, *49*, 370−378.

(16) Sassella, A.; Tubino, R.; Borghesi, A.; Giardini, M. E.; Quadrelli, L. Spectroscopic ellipsometry measurements on an anisotropic organic crystal: potassium acid phtalate. *Thin Solid Films* **1998**, *313*−*314*, 347−350.

(17) Ossó, J. O.; Schreiber, F.; Alonso, M. I.; Garriga, M.; Barrena, E.; Dosch, H. Structure, Morphology, and Optical Properties of Thin Films of F16CuPc Grown on Silicon Dioxide. *Org. Electron.* **2004**, *5*, 135−140.

(18) Hinderhofer, A.; Heinemeyer, U.; Gerlach, A.; Kowarik, S.; Jacobs, R. M. J.; Sakamoto, Y.; Suzuki, T.; Schreiber, F. Optical

DOI: 10.1021/acs.jpcc.8b03744
J. Phys. Chem. C 2018, 122, 18705−18714

Properties of Pentacene and Perfluoropentacene Thin Films. *J. Chem. Phys.* **2007**, *127*, 194705.
(19) Heinemeyer, U.; Hinderhofer, A.; Alonso, M. I.; Ossó, J. O.; Garriga, M.; Kytka, M.; Gerlach, A.; Schreiber, F. Uniaxial Anisotropy of Organic Thin Films Determined by Ellipsometry. *Phys. Status Solidi A* **2008**, *205*, 927−930.
(20) Yokoyama, D.; Sakaguchi, A.; Suzuki, M.; Adachi, C. Horizontal Molecular Orientation in Vacuum-Deposited Organic Amorphous Films of Hole and Electron Transport Materials. *Appl. Phys. Lett.* **2008**, *93*, 173302.
(21) Reisz, B.; Weimer, S.; Banerjee, R.; Zeiser, C.; Lorch, C.; Duva, G.; Dieterle, J.; Yonezawa, K.; Yang, J.-P.; Ueno, N.; et al. Structural, Optical, and Electronic Characterization of Perfluorinated Sexithiophene Films and Mixed Films with Sexithiophene. *J. Mater. Res.* **2017**, *32*, 1908−1920.
(22) Méndez, H.; Heimel, G.; Opitz, A.; Sauer, K.; Barkowski, P.; Oehzelt, M.; Soeda, J.; Okamoto, T.; Takeya, J.; Arlin, J.-B.; et al. Doping of Organic Semiconductors: Impact of Dopant Strength and Electronic Coupling. *Angew. Chem., Int. Ed.* **2013**, *52*, 7751−7755.
(23) Belova, V.; Beyer, P.; Meister, E.; Linderl, T.; Halbich, M.-U.; Gerhard, M.; Schmidt, S.; Zechel, T.; Meisel, T.; Generalov, A. V.; et al. Evidence for Anisotropic Electronic Coupling of Charge Transfer States in Weakly Interacting Organic Semiconductor Mixtures. *J. Am. Chem. Soc.* **2017**, *139*, 8474−8486.
(24) Koech, P. K.; Padmaperuma, A. B.; Wang, L.; Swensen, J. S.; Polikarpov, E.; Darsell, J. T.; Rainbolt, J. E.; Gaspar, D. J. Synthesis and Application of 1,3,4,5,7,8-Hexafluorotetracyanonaphthoquinodimethane (F6-TNAP): A Conductivity Dopant for Organic Light-Emitting Devices. *Chem. Mater.* **2010**, *22*, 3926−3932.
(25) Dürr, A. C.; Schreiber, F.; Münch, M.; Karl, N.; Krause, B.; Kruppa, V.; Dosch, H. High Structural Order in Thin Films of the Organic Semiconductor Diindenoperylene. *Appl. Phys. Lett.* **2002**, *81*, 2276−2278.
(26) Tripathi, A. K.; Pflaum, J. Correlation Between Ambipolar Transport and Structural Phase Transition in Diindenoperylene Single Crystals. *Appl. Phys. Lett.* **2006**, *89*, 082103.
(27) Heinrich, M. A.; Pflaum, J.; Tripathi, A. K.; Frey, W.; Steigerwald, M. L.; Siegrist, T. Enantiotropic Polymorphism in Diindenoperylene. *J. Phys. Chem. C* **2007**, *111*, 18878−18881.
(28) Servet, B.; Ries, S.; Trotel, M.; Alnot, P.; Horowitz, G.; Garnier, F. X-ray Determination of the Crystal Structure and Orientation of Vacuum Evaporated Sexithiophene Films. *Adv. Mater.* **1993**, *5*, 461−464.
(29) Servet, B.; Horowitz, G.; Ries, S.; Lagorsse, O.; Alnot, P.; Yassar, A.; Deloffre, F.; Srivastava, P.; Hajlaoui, R. Polymorphism and Charge Transport in Vacuum-Evaporated Sexithiophene Films. *Chem. Mater.* **1994**, *6*, 1809−1815.
(30) Horowitz, G.; Bachet, B.; Yassar, A.; Lang, P.; Demanze, F.; Fave, J.-L.; Garnier, F. Growth and Characterization of Sexithiophene Single Crystals. *Chem. Mater.* **1995**, *7*, 1337−1341.
(31) Han, W. N.; Yonezawa, K.; Makino, R.; Kato, K.; Hinderhofer, A.; Murdey, R.; Shiraishi, R.; Yoshida, H.; Sato, N.; Ueno, N.; et al. Quantitatively Identical Orientation-Dependent Ionization Energy and Electron Affinity of Diindenoperylene. *Appl. Phys. Lett.* **2013**, *103*, 253301.
(32) Duhm, S.; Heimel, G.; Salzmann, I.; Glowatzki, H.; Johnson, R. L.; Vollmer, A.; Rabe, J. P.; Koch, N. Orientation-Dependent Ionization Energies and Interface Dipoles in Ordered Molecular Assemblies. *Nat. Mater.* **2008**, *7*, 326−332.
(33) Hill, I. G.; Kahn, A.; Soos, Z. G.; Pascal, R. A., Jr Charge-separation energy in films of π-conjugated organic molecules. *Chem. Phys. Lett.* **2000**, *327*, 181−188.
(34) Siegrist, T.; Fleming, R. M.; Haddon, R. C.; Laudise, R. A.; Lovinger, A. J.; Katz, H. E.; Bridenbaugh, P.; Davis, D. D. The crystal structure of the high-temperature polymorph of α-hexathienyl (α-6T/HT). *J. Mater. Res.* **1995**, *10*, 2170−2173.
(35) Macrae, C. F.; Bruno, I. J.; Chisholm, J. A.; Edgington, P. R.; McCabe, P.; Pidcock, E.; Rodriguez-Monge, L.; Taylor, R.; van de Streek, J.; Wood, P. A. Mercury CSD 2.0- new features for the visualization and investigation of crystal structures. *J. Appl. Crystallogr.* **2008**, *41*, 466−470.
(36) Nicklin, C.; Arnold, T.; Rawle, J.; Warne, A. Diamond Beamline I07: a Beamline for Surface and Interface Diffraction. *J. Synchrotron Radiat.* **2016**, *23*, 1245−1253.
(37) Schlepütz, C. M.; Herger, R.; Willmott, P. R.; Patterson, B. D.; Bunk, O.; Brönnimann, C.; Henrich, B.; Hülsen, G.; Eikenberry, E. F. Improved Data Acquisition in Grazing-Incidence X-ray Scattering Experiments Using a Pixel Detector. *Acta Crystallogr., Sect. A: Found. Crystallogr.* **2005**, *61*, 418−425.
(38) Florence, J. M.; Allshouse, C. C.; Glaze, F. W.; Hahner, C. H. Absorption of Near-Infrared Energy by Certain Glasses. *J. Res. Natl. Bur. Stand.* **1950**, *45*, 121.
(39) Woollam, J. A. *Guide to Using WVASE. Spectroscopic Ellipsometry Data Acquisition and Analysis Software*; J. A. Woollam Co., Inc., 2012.
(40) Hu, P.; Wang, S.; Chaturvedi, A.; Wei, F.; Zhu, X.; Zhang, X.; Li, R.; Li, Y.; Jiang, H.; Long, Y.; et al. Impact of C-H···X (X = F, N) and π-π Interactions on Tuning the Degree of Charge Transfer in F6TNAP-Based Organic Binary Compound Single Crystals. *Cryst. Growth Des.* **2018**, *18*, 1776−1785.
(41) Lorch, C.; Novák, J.; Banerjee, R.; Weimer, S.; Dieterle, J.; Frank, C.; Hinderhofer, A.; Gerlach, A.; Carla, F.; Schreiber, F. Influence of C60 co-deposition on the growth kinetics of diindenoperylene-From rapid roughening to layer-by-layer growth in blended organic films. *J. Chem. Phys.* **2017**, *146*, 052807.
(42) Banerjee, R.; Novák, J.; Frank, C.; Lorch, C.; Hinderhofer, A.; Gerlach, A.; Schreiber, F. Evidence for Kinetically Limited Thickness Dependent Phase Separation in Organic Thin Film Blends. *Phys. Rev. Lett.* **2013**, *110*, 185506.
(43) Moser, A.; Salzmann, I.; Oehzelt, M.; Neuhold, A.; Flesch, H.-G.; Ivanco, J.; Pop, S.; Toader, T.; Zahn, D. R. T.; Smilgies, D.-M.; et al. A Disordered Layered Phase in Thin Films of Sexithiophene. *Chem. Phys. Lett.* **2013**, *574*, 51−55.
(44) Lorch, C.; Banerjee, R.; Frank, C.; Dieterle, J.; Hinderhofer, A.; Gerlach, A.; Schreiber, F. Growth of Competing Crystal Phases of α-Sexithiophene Studied by Real-Time in Situ X-ray Scattering. *J. Phys. Chem. C* **2015**, *119*, 819−825.
(45) Mahns, B.; Kataeva, O.; Islamov, D.; Hampel, S.; Steckel, F.; Hess, C.; Knupfer, M.; Büchner, B.; Himcinschi, C.; Hahn, T.; et al. Crystal Growth, Structure, and Transport Properties of the Charge-Transfer Salt Picene/2,3,5,6-Tetrafluoro-7,7,8,8-Tetracyanoquinodimethane. *Cryst. Growth Des.* **2014**, *14*, 1338−1346.
(46) Hotta, S.; Kobayashi, H. Crystal and molecular structure of a charge-transfer complex between α,α′-dimethylquaterthiophene and 2,3,5,6-tetrafluoro-7,7,8,8-tetracyanoquinodimethane. *Synth. Met.* **1994**, *66*, 117−122.
(47) Emge, T. J.; Bryden, W. A.; Wiygul, F. M.; Cowan, D. O.; Kistenmacher, T. J.; Bloch, A. N. Structure of an organic charge-transfer salt derived from dibenzotetrathiafulvalene and tetrafluorotetracyanoquinodimethane (DBTTF-TCNQF4). Observation of a high-temperature phase transition. *J. Chem. Phys.* **1982**, *77*, 3188−3197.
(48) Hu, P.; Li, H.; Li, Y.; Jiang, H.; Kloc, C. Single-Crystal Growth, Structures, Charge Transfer and Transport Properties of Anthracene-F4TCNQ and Tetracene-F4TCNQ Charge-Transfer Compounds. *CrystEngComm* **2017**, *19*, 618−624.
(49) Hlawacek, G.; Puschnig, P.; Frank, P.; Winkler, A.; Ambrosch-Draxl, C.; Teichert, C. Characterization of Step-Edge Barriers in Organic Thin-Film Growth. *Science* **2008**, *321*, 108−111.
(50) Porzio, W.; Destri, S.; Mascherpa, M.; Brückner, S. Structural Aspects of Oligothienyl Series from X-ray Powder Diffraction Data. *Acta Polym.* **1993**, *44*, 266−272.
(51) Reinhardt, J. P.; Hinderhofer, A.; Broch, K.; Heinemeyer, U.; Kowarik, S.; Vorobiev, A.; Gerlach, A.; Schreiber, F. Structural and Optical Properties of Mixed Diindenoperylene-Perfluoropentacene Thin Films. *J. Phys. Chem. C* **2012**, *116*, 10917−10923.
(52) Greiner, D.; Hinrichs, V.; Wiesner, S.; Ludwig, W.; Fostiropoulos, K.; Keiper, D.; Baumann, P. K.; Meyer, N.; Heuken, M.; Rusu, M.; et al. Optical Constants of Diindenoperylene in the

DOI: 10.1021/acs.jpcc.8b03744
J. Phys. Chem. C 2018, 122, 18705−18714

Dependence of Preparation Temperature and Pressure. *Thin Solid Films* **2013**, *534*, 255−259.
(53) Opitz, A.; Banerjee, R.; Grob, S.; Gruber, M.; Hinderhofer, A.; Hörmann, U.; Kraus, J.; Linderl, T.; Lorch, C.; Steindamm, A.; et al. *Elementary Processes in Organic Photovoltaics*; Leo, K., Ed.; Springer International Publishing: Cham, 2017; pp 77−108.
(54) Goetz, K. P.; Tsutsumi, J.; Pookpanratana, S.; Chen, J.; Corbin, N. S.; Behera, R. K.; Coropceanu, V.; Richter, C. A.; Hacker, C. A.; Hasegawa, T.; et al. Polymorphism in the 1:1 Charge-Transfer Complex DBTTF-TCNQ and Its Effects on Optical and Electronic Properties. *Adv. Electron. Mater.* **2016**, *2*, 1600203.
(55) Girlando, A. Comment on Polymorphism in the 1:1 Charge-Transfer Complex DBTT-TCNQ and Its Effects on Optical and Electronic Properties. *Adv. Electron. Mater.* **2017**, *3*, 1600437.
(56) Goetz, K. P.; Tsutsumi, J.; Pookpanratana, S.; Chen, J.; Corbin, N. S.; Behera, R. K.; Coropceanu, V.; Richter, C. A.; Hacker, C. A.; Hasegawa, T.; et al. Reply to Comment on Polymorphism in the 1:1 Charge-Transfer Complex DBTTF-TCNQ and Its Effects on Optical and Electronic Properties. *Adv. Electron. Mater.* **2017**, *3*, 1600521.
(57) Broch, K.; Heinemeyer, U.; Hinderhofer, A.; Anger, F.; Scholz, R.; Gerlach, A.; Schreiber, F. Optical Evidence for Intermolecular Coupling in Mixed Films of Pentacene and Perfluoropentacene. *Phys. Rev. B: Condens. Matter Mater. Phys.* **2011**, *83*, 245307.
(58) Zhang, Q.; Liu, X.; Jiao, F.; Braun, S.; Jafari, M. J.; Crispin, X.; Ederth, T.; Fahlman, M. Ground-State Charge Transfer for NIR Absorption with Donor/Acceptor Molecules: Interactions Mediated via Energetics and Orbital Symmetries. *J. Mater. Chem. C* **2017**, *5*, 275−281.
(59) Braun, K.-F.; Hla, S. W. Charge Transfer in the TCNQ-Sexithiophene Complex. *J. Chem. Phys.* **2008**, *129*, 064707.
(60) Karpov, Y.; Erdmann, T.; Stamm, M.; Lappan, U.; Guskova, O.; Malanin, M.; Raguzin, I.; Beryozkina, T.; Bakulev, V.; Günther, F.; et al. Molecular Doping of a High Mobility Diketopyrrolopyrrole-Dithienylthieno[3,2-b]thiophene Donor-Acceptor Copolymer with F6TCNNQ. *Macromolecules* **2017**, *50*, 914−926.
(61) Lane, P. A.; Wei, X.; Vardeny, Z. V.; Poplawski, J.; Ehrenfreund, E.; Ibrahim, M.; Frank, A. J. Absorption spectroscopy of charged excitations in α-sexithiophene: evidence for charge conjugation symmetry breaking. *Chem. Phys.* **1996**, *210*, 229−234.

DOI: 10.1021/acs.jpcc.8b03744
J. Phys. Chem. C 2018, 122, 18705−18714